



**Michigan
Technological
University**

Michigan Technological University
Digital Commons @ Michigan Tech

Department of Physics Publications

Department of Physics

5-21-2017

Terrestrial glint seen from deep space: Oriented ice crystals detected from the Lagrangian point

Alexander Marshak
NASA Goddard Space Flight Center

Tamas Varnai
University of Maryland - Baltimore County

Alexander Kostinski
Michigan Technological University

Follow this and additional works at: <https://digitalcommons.mtu.edu/physics-fp>


 Part of the [Physics Commons](#)

Recommended Citation

Marshak, A., Varnai, T., & Kostinski, A. (2017). Terrestrial glint seen from deep space: Oriented ice crystals detected from the Lagrangian point. *Geophysical Research Letters*, 44(10), 5197-5202. <http://dx.doi.org/10.1002/2017GL073248>

Retrieved from: <https://digitalcommons.mtu.edu/physics-fp/166>

Follow this and additional works at: <https://digitalcommons.mtu.edu/physics-fp>

 Part of the [Physics Commons](#)



RESEARCH LETTER

10.1002/2017GL073248

Key Points:

- Colorful bright flashes over land detected in the DSCOVR images come from glint off horizontally oriented ice crystals in cirrus clouds
- Deep space detection of tropospheric ice can help constrain the likelihood of oriented ice crystals and their contribution to Earth albedo
- Deep space detection of sun glints off faint companions can be used in our search for habitable exoplanets

Correspondence to:

A. Marshak

alexander.marshak@nasa.gov

Citation:

Marshak, A., T. Várnai, and A. Kostinski (2017), Terrestrial glint seen from deep space: Oriented ice crystals detected from the Lagrangian point, *Geophys. Res. Lett.*, 44, 5197–5202, doi:10.1002/2017GL073248.

Received 24 FEB 2017

Accepted 1 MAY 2017

Accepted article online 15 MAY 2017

Published online 21 MAY 2017

Published 2017. This article is a US Government work and is in the public domain in the United States of America.

Terrestrial glint seen from deep space: Oriented ice crystals detected from the Lagrangian point

Alexander Marshak¹ , Tamás Várnai^{1,2}, and Alexander Kostinski³ 

¹NASA Goddard Space Flight Center, Greenbelt, Maryland, USA, ²Joint Center for Earth Systems Technology, University of Maryland, Baltimore County, Baltimore, Maryland, USA, ³Department of Physics, Michigan Technological University, Houghton, Michigan, USA

Abstract The Deep Space Climate Observatory (DSCOVR) spacecraft resides at the first Lagrangian point about one million miles from Earth. A polychromatic imaging camera onboard delivers nearly hourly observations of the entire sunlit face of the Earth. Many images contain unexpected bright flashes of light over both ocean and land. We construct a yearlong time series of flash latitudes, scattering angles, and oxygen absorption to demonstrate conclusively that the flashes over land are specular reflections off tiny ice platelets floating in the air nearly horizontally. Such deep space detection of tropospheric ice can be used to constrain the likelihood of oriented crystals and their contribution to Earth albedo. These glint observations also support proposals for detecting starlight glints off faint companions in our search for habitable exoplanets.

Plain Language Summary The Deep Space Climate Observatory (DSCOVR) spacecraft resides at the first Lagrangian point about one million miles from Earth. An imaging camera onboard delivers nearly hourly observations of the entire sunlit face of the Earth. Many images contain unexpected bright flashes of light over both ocean and land. We construct a yearlong time series of flash latitudes, scattering angles, and oxygen absorption to demonstrate conclusively that the flashes over land are specular reflections off tiny ice platelets floating in the air nearly horizontally. Such deep space detection of tropospheric ice can be used to constrain the likelihood of oriented crystals and their contribution to Earth albedo. These glint observations also support proposals for detecting starlight glints off faint companions in our search for habitable exoplanets.

1. Introduction

In 1993 *Sagan et al.* [1993] used the spacecraft Galileo flyby observation of Earth as a control experiment in search for life elsewhere [*Sagan et al.*, 1993]. On page 718 they noted "... close examination of the images shows a region of specular reflection in ocean but not on land". However, we found specular reflections (glints) over land in the Galileo images of Earth. [The movie (courtesy of NASA/JPL) at <https://www.youtube.com/watch?v=ceJOBfj3hKs> shows the view of Earth from 2.08 million kilometer distance, captured by the Jupiter-bound space probe Galileo on 11 December 1990. Sun glint over land is clearly seen in the very first second over Brazil.]

We conjectured glints off horizontally oriented ice platelets floating in cirrus clouds as the physical origin but lacked proof. Meanwhile, the Earth Polychromatic Imaging Camera (EPIC) on board the Deep Space Climate Observatory (DSCOVR) spacecraft arrived at the first Lagrangian point (L1) a million miles (1.5 million km) away in June 2015 and has been in orbit since then. Serendipitously, not only has it detected the bright flashes over land but it has also accorded us an opportunity to prove that glint off horizontally floating ice platelets in clouds is indeed the physical origin of distant flashes. In this paper we explain the observational evidence for this hypothesis.

2. Data and Methods

EPIC is a 10-channel spectroradiometer (317–780 nm), taking 10 narrow band spectral images of the entire sunlit face of Earth approximately every hour (from mid-April to mid-October) or every 2 h (rest of the year) using a 2048 × 2048 pixel charge-coupled device (CCD). The pixel size projected onto the Earth near the image center is about 10 × 10 km², and the angular spread is ~3 × 10⁻⁴ degree. Because EPIC uses a rotating filter wheel, there is a time lag between the images at different wavelengths: ~3 min difference between blue (443 nm) and green (551 nm), ~4 min between blue and red (680 nm). The true-color (red-green-blue) images

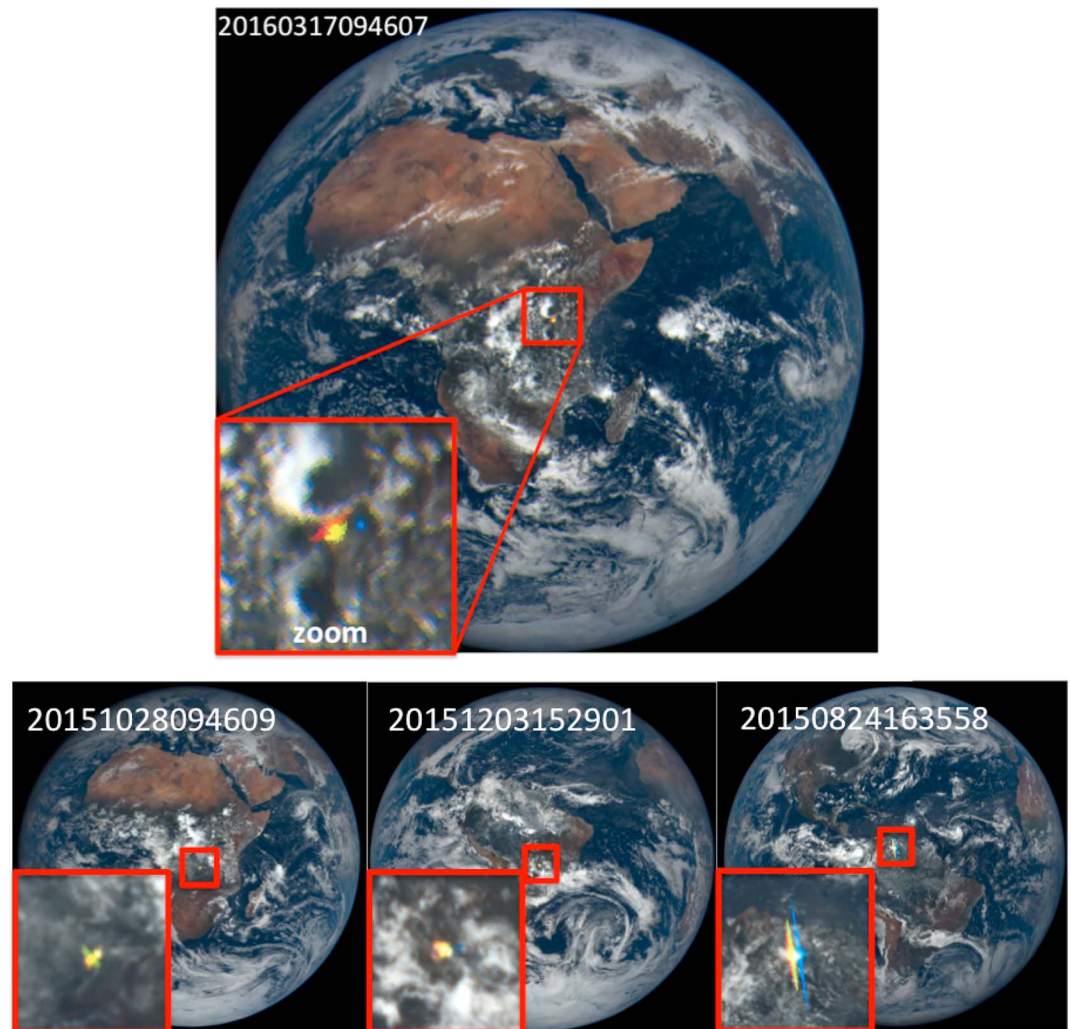


Figure 1. Examples of terrestrial glint. The dates and times when these true-color composite images were captured are shown at the top left corner of each image. For example, the top image was obtained on 17 March 2016 around 9:46 UTC. All EPIC true-color images are available at <http://epic.gsfc.nasa.gov>. The pixel size is about $10 \times 10 \text{ km}^2$. A wheel inside EPIC spins color filters, causing a time lag between the component images: ~ 3 min between blue (443 nm) and green (551 nm), ~ 4 min between blue and red (680 nm). The framed regions contain bright colorful spots discernible by a naked eye (magnified in the insets). The physical origin of such bright flashes over land is shown in Figures 2 and 3 to be the glint off ice crystals in cirrus clouds.

are generated daily and are available at <http://epic.gsfc.nasa.gov>. Many of the images collected over the 400 days contain the conspicuous variously colored bright spots over land as well as over water; a few examples over land are shown in Figure 1.

In order to test the hypothesis that the detected bright flashes are caused by specular reflection from horizontally oriented crystals in ice clouds, we compiled a roughly yearlong data set of EPIC images. We then developed an automated algorithm to identify glints over land via reflectance ratios at different wavelengths (R_{443}/R_{680} , R_{551}/R_{443} , and R_{680}/R_{443}). These ratios are high for glint pixels because blue images are taken 3–4 min before red and green images, and during this time the Earth rotation shifts the glint positions. The detection algorithm consists of the following steps:

1. (Preliminary): Eliminate EPIC *images* where data for any of the 10 EPIC bands is missing.
2. (Glint vicinity): Eliminate *pixels* where the deviation from the exact specular reflection angle is larger than 5° .
3. (Land only): Eliminate *pixels* where a global map of surface types indicates the presence of water, snow, or ice surfaces within ~ 20 km in each direction. The 20 km buffer zone serves as safety cushion against errors in EPIC geolocation or in the surface type map.

4. (Color ratio): Eliminate pixels with color ratio (CR) below a certain threshold. The CR is calculated as

$$CR_{443}(i, j) = R_{443}(i, j) / R_{680}^{\max}(i, j)$$

for detecting glints in *blue* images;

$$CR_{551}(i, j) = R_{551}(i, j) / R_{443}^{\max}(i, j)$$

for detecting glints in *green* images; and

$$CR_{680}(i, j) = R_{680}(i, j) / R_{443}^{\max}(i, j)$$

for detecting glints in *red* images. Here

$$R_{\lambda}^{\max}(i, j) = \max_{\substack{i-1 \leq m \leq i+1 \\ j-1 \leq n \leq j+1}} R_{\lambda}(m, n).$$

We divide by the maximum reflectance of 3×3 pixel areas in order to avoid false positives at pixels that appear colorful only because clouds moved in or out of the pixel area during the 3–4 min between the acquisition of blue and green (or red) images.

The CR threshold for glint detection is a function of reflectance at the “reference wavelength” used in the denominator when calculating the CR. For each reference band reflectance value, the threshold is chosen such that most pixels whose deviation from the exact specular reflection angle is in the 5° – 15° range will have CRs lower than the chosen threshold value. This implies that CRs above this threshold are exceedingly rare unless due to specular reflection.

5. (Green or red): In searching for green glints, eliminate pixels for which $R_{680} > R_{551}$. In searching for red glints, eliminate pixels for which $R_{551} > R_{680}$. (Most of the green glints have a high enough red reflectance to appear yellow rather than green.)

Finally, all pixels not eliminated during this five-step process are declared *glint pixels*.

Note that bright glints can cause “wings” to appear due to instrument effects (for example, in the bottom right of Figure 1). Such wings occur because each pixel in the EPIC detector array can store only a finite number of electrons, and any extra electrons are spread over the column containing the saturated pixel (see https://www.eso.org/~ohainaut/ccd/CCD_artifacts.html). Our analysis does not depend on this saturation effect.

3. Results

Scanning all images from June 2015 to August 2016, the automated algorithm described above detected 213 red, 336 blue, and 317 green flashes. What is the origin of these flashes, e.g., could these be lighting strikes? Figure 2 (left) compares the measured latitudes of the detected bright colorful flashes (marked by colorful spots) with the theoretical ones that permit specular reflection for a given time of year and color (gray curve).

The black band inset displays the geographical locations of flashes for the three colors and shows a rather random distribution within the available area. As the Earth’s axial tilt (23.4°) causes local zenith directions to vary, the location of flashes reaches its southernmost latitude of $\sim 25^{\circ}$ S around 22 December and its northernmost latitude of $\sim 25^{\circ}$ N around 22 June. The detected flashes are near the equator around the equinoxes in March and September. The almost complete coincidence of the measured latitudes for all three colors, 866 points in all, with the gray theoretical curve of latitudes that permit specular reflection as a function of time, constitutes compelling evidence for the glint hypothesis and rules out nonspecular sources such as lightning.

To further test the glint conjecture, Figure 2 (right) compares the sum of solar zenith angle (SZA) and vehicle zenith angle (VZA) with the Sun-Earth-Vehicle (SEV) vertex angle (left and right y axis, respectively). The zenith direction is along the normal to a given pixel at the Earth surface, but the three vectors do not necessarily lie in the same plane. In other words, the SEV triangle does not necessarily contain the normal (zenith) vector. A necessary and sufficient condition for coplanarity and specular reflection is $SZA + VZA = SEV$. To that end, the gray curve plotted in Figure 2 (right) is a set of angles such that specular reflection can occur, per given time of year and color. Once again, the agreement is quite good and further confirms the specular reflection hypothesis.

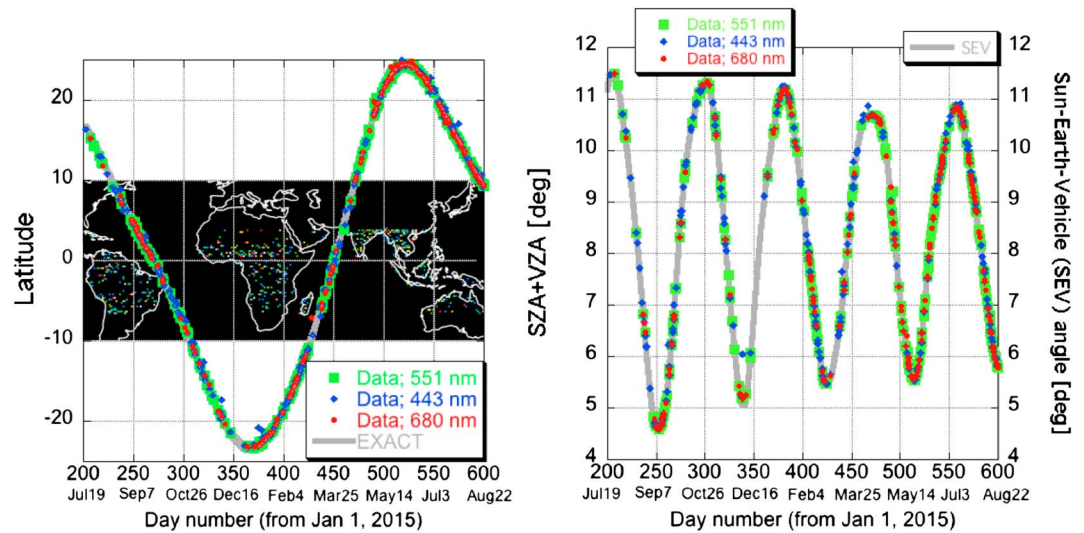


Figure 2. Evidence for the Specular Reflection Hypothesis. (left) Gray curve is a set of latitudes that permit specular reflection for a given time of year and color. The measured glint latitudes for each color are also shown, and it is seen that all data points fall within or next to the specular reflection curve. Map in black band: locations of glints. (right) The sum of solar zenith angle (SZA) and vehicle zenith angle (VZA) plotted along with the Sun-Earth-Vehicle (SEV) vertex angle (left and right y axis, respectively). A necessary and sufficient condition for coplanarity and specular reflection is $SZA + VZA = SEV$. The gray curve is a set of angles that permit specular reflection for a given time of year and color. The constructed time series of measured glint angles for each color fall within or next to the specular reflection curve. This confirms the specular reflection hypothesis.

While evidence presented in Figure 2 for the specular reflection conjecture over land is compelling and points to clouds as a likely cause, independent proof for the ice cloud origin of the glints is sought. To that end, we turn to EPIC measurements of absorption by molecular oxygen (O_2) via the ratio of absorbing channel (764 and 688 nm, A and B bands, respectively) reflectances to adjacent nonabsorbing channel (780 and 680 nm) reflectances. This ratio is used to estimate cloud height, as it is higher when high clouds prevent sunlight from reaching the lower atmosphere, where more O_2 absorption would occur [e.g., *Heidinger and Stephens, 2000*]. Note that the time difference between the red (680 nm) and the O_2 B band (688 nm) and between the NIR (780 nm) and the O_2 A band (764 nm) is only 27 s.

Figure 3 (left) shows that for blue glints, the histograms for A and B band ratios peak at 0.37 and 0.68, respectively. Figure 3 (right) shows radiative transfer simulations of A and B band ratios, mimicking the EPIC bands and the light scattering geometry for cloud optical depths (τ) = 1, 3, and 5 over vegetated areas. Thin clouds with τ between 1 and 3 yield intersections with the solid gray lines at cloud heights of 5–8 km. Cloud heights greater than 5 km practically ensure ice phase. Hence, cloud ice platelets are responsible for the glints. Note that $\tau = 1$ corresponds to a cloud whose thickness is equal to a photon mean-free path, and specular (hence, single) scattering is dominant.

4. Discussion

While we are not aware of deep space observations of glint off tropospheric ice clouds, atmospheric observations of such specular reflections have been made via regular photography from the ground [*Lynch et al., 1994*] and onboard aircraft [*Lynch and Livingston, 2001, p. 160*], with ground-based lidars [*Sassen and Benson, 2001*] and by satellites on low-Earth orbit: POLDER (Polarization and Directionality of the Earth's Reflectances) polarized measurements [*Chepfer et al., 1999; Breon and Dubrulle, 2004; Noel and Chepfer, 2004*] and CALIPSO (Cloud-Aerosol Lidar and Infrared Pathfinder Satellite Observation) lidar returns [*Noel and Chepfer, 2010*]. All such glint observations are bounded by an altitude of about 700 km and have broader angular resolution than EPIC. The geometric mean distance of POLDER/CALIPSO and EPIC observations is about the distance of geostationary orbit (36,000 km) but, to the best of our knowledge, there have been no glint observations there. Thus, the distance of terrestrial glint observations reported here exceed the

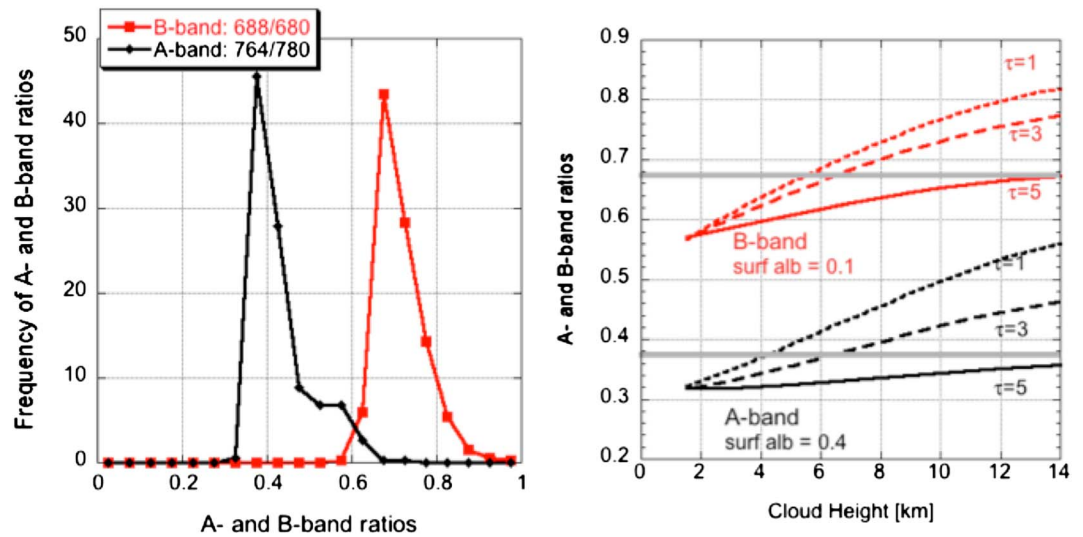


Figure 3. Evidence for the ice cloud origin of the glints. While evidence presented in Figure 2 confirms specular reflection over land, identifying the source as ice platelets inside clouds requires confirmation. To that end, we turn to EPIC measurements of absorption by molecular oxygen (O_2) via the ratio of absorbing (764 and 688 nm) to nonabsorbing (780 and 680 nm) channel reflectances (A and B bands). (left) The histograms for blue glints, peak at 0.37 and 0.68, for A and B bands, respectively. (right) Radiative transfer simulations of EPIC A and B band ratios, assuming SZA = VZA = 5°; SEV = 8°; cloud thickness = 1 km; ice crystal size with effective radius = 20 μm ; surface albedo = 0.4 and 0.1 for A band and B band, respectively; and cloud optical depths (τ) = 1, 3, and 5. The horizontal gray lines mark the ratio values that are most often observed in glint areas. Dashed lines for τ between 1 and 3 over vegetated areas intersect the gray lines at cloud heights of 5–8 km, indicating that the glints occur at medium-high clouds that are most likely to contain horizontally oriented ice platelets.

range of prior glint observations by over 3 orders of magnitude and serve as a milestone on the road from typical Earth remote sensing to the detection of starlight glint off exoplanets [Williams and Gaidos, 2008; Robinson et al., 2010, Borovoi et al., 2012].

Based on in situ measurements of cirrus clouds, [Korolev et al., 2000; McFarquhar et al., 2002], tiny hexagonal platelets of ice, floating in air in nearly perfect horizontal alignment, are likely responsible for the glints observed by EPIC over land. Because the EPIC instrument has a field of view of 0.62° (see <https://epic.gsfc.nasa.gov/epic>) and a 2048×2048 pixels CCD, the specular signal within an angle of only $\sim 3 \times 10^{-4}$ degree (Figure 2) must either contain smooth large-oriented ice plates or smaller-oriented platelets sending back diffracted light. Size distribution of such crystals depends greatly on cloud temperature and humidity, but the range is from tens of microns to microns. Taking the wavelength of $0.5 \mu\text{m}$ and ice platelet size of $50 \mu\text{m}$ yields the ratio or angular half width of the diffraction lobe around the specular direction 10^{-2} or on the order of a degree [Crawford, 1968, p. 486]. This is broader than the angular width of a pixel but narrower than change in the zenith direction over the area covered by a pixel (0.1°). This implies that the previously invoked large, wobbling millimeter-sized crystals, [e.g., Chepfer et al., 1999] are not the only explanation, and glints with observed angular spread of about a degree can also be explained by the simple diffraction estimate. Disentangling the diffraction effects from orientation distribution, using EPIC’s unique vantage point is likely to yield unexpected insights into changes in Earth albedo.

Out of total 4106 images collected, 336 contain land glint for the blue channel, which was chosen because it has the highest spatial resolution (to reduce the amount of data transmitted from DSCOVR, for all other channels, four pixels are averaged on board the spacecraft). Can one interpret this ratio $336/4106 = 8.2\%$? To exclude images with ocean at the location of possible glint, we divide the 8.2% by the land fraction in EPIC tropical band (1/4), yielding 32.8%. Hence, roughly one in three images with land in the center contains a glint from an ice cloud. This matches the fraction of Earth covered by ice clouds in tropics which is also about a third [King et al., 2013]. This agreement suggests that terrestrial glints seen from deep space supply efficient means of detecting cloud ice, reflecting at least a factor of 5–6 stronger than surrounding pixels, and may substantially increase cloud albedo [Takano and Liou, 1989], relative to diffuse reflectance from randomly

oriented ice particles. This is significant as cirrus clouds, composed mostly of aspherical particles, cover over 30% of the Earth surface and play a major role in the radiation budget [Stephens *et al.*, 1990].

The EPIC detectors report a photon flux count on the order of $10^5/s$ (10^2 – 10^3 W/m²/μm/sr, depending on wavelength) for glint pixels even for optically thin cirrus clouds. Thus, much like a human eye, the distant Lagrangian eye readily registers a glint signal. Such detection of relatively feeble light based on contrast renders starlight glint off faint companions feasible. Glints have figured prominently in many fields, e.g., the celebrated work on measuring sea surface roughness in oceanography [Cox and Munk, 1954] and now may span the gamut from atmospheric science to exoplanet research.

Acknowledgments

This research was supported by the NASA DSCOVR project and by NSF AGS-1639868. We thank Y. Yang for helping with EPIC O₂ simulations and K. Blank and J. Herman for helping us better understand EPIC Level 1 data. We also thank P. Yang and B. van Diedenhoven for insightful discussions on the nature of the subsuns and cloud microphysical processes. Finally, we would like to acknowledge G.S. Hernandez for the help with visual analysis of EPIC images. The EPIC data were obtained from the NASA Langley Research Center Atmospheric Science Data Center (https://eosweb.larc.nasa.gov/project/dscovr/dscovr_table).

References

- Borovoi, A., A. Konoshonkin, and L. Kolokolova (2012), Glints from particulate media and wavy surfaces, *J. Quant. Spectrosc. Radiat. Transfer*, *113*, 2542–2551.
- Breon, F.-M., and B. Dubrulle (2004), Horizontally oriented plates in clouds, *J. Atm. Sci.*, *61*, 2888–2898.
- Chepfer, H., G. Brogniez, P. Goloub, F. M. Breon, and P. H. Flamant (1999), Observations of horizontally oriented ice crystals in cirrus clouds with POLDER-1/ADEOS-1, *J. Quant. Spectrosc. Radiat. Transfer*, *63*, 521–543.
- Cox, C., and W. Munk (1954), Measurement of the roughness of the sea surface from photographs of the Sun's glitter, *J. Opt. Soc. Am.*, *44*, 838–850.
- Crawford, F. (1968), *Waves: Berkeley Physics Course*, vol. 3, 600 pp., McGraw-Hill, Berkeley, Calif.
- Heidinger, A. K., and G. L. Stephens (2000), Molecular line absorption in a scattering atmosphere. II: Application to remote sensing in the O₂ A-band, *J. Atmos. Sci.*, *57*, 1615–1634.
- King, M. D., S. Platnick, W. P. Menzel, S. A. Ackerman, and P. A. Hubanks (2013), Spatial and temporal distribution of clouds observed by MODIS onboard the Terra and Aqua satellites, *IEEE Trans. Geosci. Remote Sens.*, *51*, 3826–3852.
- Korolev, A., G. A. Isaac, and J. Hallett (2000), Ice particle habits in stratiform clouds, *Q. J. R. Meteorol. Soc.*, *126*, 2873–2902.
- Lynch, D. K., and W. Livingston (2001), *Color and Light in Nature*, 2nd ed., 292 pp., Cambridge Univ. Press, Cambridge, U. K.
- Lynch, D. K., S. D. Gedzelman, and A. B. Fraser (1994), Subsuns, Bottlinger's rings and elliptical halos, *Appl. Opt.*, *33*, 4580–4589.
- McFarquhar, G. M., P. Yang, A. Macke, and A. J. Baran (2002), A new parameterization of single scattering solar radiative properties for tropical anvils using observed ice crystal size and shape distributions, *J. Atmos. Sci.*, *59*, 2458–2478.
- Noel, V., and H. Chepfer (2004), Study of ice crystal orientation in cirrus clouds based on satellite polarized radiance measurements, *J. Atmos. Sci.*, *61*, 2073–2081.
- Noel, V., and H. Chepfer (2010), A global view of horizontally oriented crystals in ice clouds from Cloud-Aerosol Lidar and Infrared Pathfinder Satellite Observation (CALIPSO), *J. Geophys. Res.*, *115*, D00H23, doi:10.1029/2009JD012365.
- Robinson, T. D., V. S. Meadows, and D. Crisp (2010), Detecting oceans on extrasolar planets using glint effect, *Astrophys. J. Lett.*, *721*, L67–L71.
- Sagan, C., W. R. Thompson, R. Carlson, D. Gurnett, and C. Hord (1993), A search for life on Earth from the Galileo spacecraft, *Nature*, *365*, 715–721.
- Sassen, K., and S. Benson (2001), A midlatitude cirrus cloud climatology from the facility for atmospheric remote sensing. Part II: Microphysical properties derived from lidar depolarization, *J. Atmos. Sci.*, *58*, 2103–2112.
- Stephens, G. L., S. C. Tsay, P. W. Stackhouse Jr., and P. J. Flateau (1990), The relevance of the microphysical and radiative properties of cirrus clouds to the climate and climatic feedback, *J. Atmos. Sci.*, *47*, 1742–1753.
- Takano, Y., and K. N. Liou (1989), Solar radiative transfer in cirrus clouds. Part II: Theory and computation of multiple scattering in an anisotropic medium, *J. Atmos. Sci.*, *46*, 20–36.
- Williams, D. M., and E. Gaidos (2008), Detecting the glint of starlight on the oceans of distant planets, *Icarus*, *195*, 927–936.